Experimental Mechanics (2014) 54:1395–1410
DOI 10.1007/s11340-014-9903-1

General Anisotropy Identification of Paperboard with Virtual Fields Method

J.M. Considine · F. Pierron · K.T. Turner · D.W. Vahey

Received: 10 December 2013 / Accepted: 8 May 2014 / Published online: 1 August 2014

Abstract This work extends previous efforts in plate bending of Virtual Fields Method (VFM) parameter identification to include a general 2-D anisotropic material. Such an extension was needed for instances in which material principal directions are unknown or when specimen orientation is not aligned with material principal directions. A new fixture with a multi-axial force configuration is introduced to provide full-field strain data for identification of the six anisotropic stiffnesses. Two paper materials were tested and their Q_{ij} compared favorably with those determined by ultrasonic and tensile tests. Accuracy of VFM identification was also quantified by variance of stiffnesses. The load fixture and VFM provide an alternative stiffness identification tool for a wide variety of thin materials to more accurately determine Q_{12} and Q_{66}.

Keywords Virtual fields method (VFM) · Digital image correlation (DIC) · Stiffness · Paperboard · Anisotropy

Introduction

Paper, paperboard, and other cellulose fiber composites have received significant attention for use in materials and structures where biocompatibility is an important consideration because cellulose fiber composites are renewable, recyclable and compostable. However, even though single-sheet papermaking is more than 4,000 years old and modern papermaking is 200 years old, analysis of paper's engineering properties remains a significant research area.

Production of paper and paperboard includes the separation of cellulose fibers, which are themselves anisotropic [1], from wood through a pulping process, which may be mechanical, as in newsprint, or chemical, as in sack paper. Resulting fiber flexibility and inter-fiber bonding are improved through an additional mechanical action called beating. Absent requirements for fiber bleaching, the fibers are dispersed at low concentrations, usually less than 1 % fiber/water,prior to being sprayed on a moving screen. Travel direction of the screen is called the machine direction (MD) while the in-plane direction perpendicular to the travel direction is called the cross-machine direction (CD). A combination of the spraying action and screen travel tend to orient the fibers in the MD, which usually corresponds with the 1-direction of material properties. Depending on the type of paper produced paper machines can operate at speeds of 1,500 m/min or higher. While ratios vary, the typical ratio for E_{11}/E_{22} is near 2. Offline stiffness measurement is used in process control [2]. Paper and paperboard are frequently sold on a strength/weight or stiffness/weight basis and so reduction of property variability and mechanical property improvement are persistent goals of papermakers, even though costs associated with variability are rarely acknowledged [3].

Paper and paperboard are hydrogen-bonded polymers which exhibit hygro-thermal, viscoelastic and plastic behaviors. Below their plastic limit their mechanical properties are considered to be linear elastic. Yeh et al. [4] made a comprehensive examination of the effect of moisture on the orthotropy, elastic moduli, Poisson's ratios, shear moduli and strain energy density. The materials in that work were linear elastic for MD and CD strains below ~1 %. A comprehensive review of properties related to moisture and viscoelasticity is found in [5]. Castro and Ostoja-Starzewski [6] examined

J. Considine (✉) · D. Vahey
US Forest Service, Forest Products Laboratory, One Gifford Pinchot Drive, Madison, WI 53726, USA
e-mail: jconsidine@fs.fed.us

F. Pierron
University of Southampton, Southampton SO17 1BJ, UK

K. Turner
University of Pennsylvania, Philadelphia, PA 19104-6315, USA

paper plasticity at a single moisture level and found linear elastic behavior below 0.5 % strain.

The objective of this work was to develop a load fixture and analysis method to identify the anisotropic stiffnesses of paper, paperboard, and other thin materials. Whereas the paper industry considers paper to be an orthotropic material, general anisotropy is developed if the MD is not aligned with the 1-direction and is called 'rotated orthotropy.' The assumption of orthotropy requires confirmation, as the papermaking process has many variables affecting sheet mechanical properties including fiber properties, fiber orientation [7], fiber length distributions, sheet density, and drying restraint [8, 9]. Finally, identification of Q_{ij}, the in-plane stiffnesses, is important for process control [10] and for structures made from paper and paperboard, e.g., corrugated fiberboard [11], wound cores [12] and paper/foil composites [13]. Additionally, anisotropic Q_{ij} identification is important for other thin materials, including surgical meshes [14], biological tissues [15], textiles [16], and rubber [17], among many others.

Identification of a fully populated Q_{ij} matrix requires a specimen and load configuration in which heterogeneous strain fields of each ε_1, ε_2, and ε_6, are developed. Several methods have been proposed for creating those heterogeneous fields, such as uniaxial tensile coupons cut in different orientations [18], uniaxial tensile coupons with a central hole [19], cruciform [20], bulge tests [21], and thin-walled cylindrical tubes [22]. Each of these specimens and load configurations had some aspect which made them unsuitable for the current work. For example, identification using uniaxial tensile specimens would require many specimens to develop statistical certainty of identification; other configurations would cause specimen wrinkling. Some specimens, such as cruciform specimens with and without central holes have stress concentrations at corners and/or holes where nonlinear constitutive behavior may be present. Small aspect-ratio tensile and bulge tests are incapable of producing different principal stress ratios. Tube configurations are complicated by a joining seam and the difficulty of full-field examination.

While application of VFM to thin materials is new, other cellulose-fiber based materials have been examined with VFM. Xavier et al. [23, 24] used the unnotched Iosipescu geometry to identify the orthotropic Q_{ij} in maritime pine wood. Le Magorou et al. [25] and Xavier et al. [26] identified plate bending stiffnesses in plywood and medium density fiberboard, respectively.

Most of the these geometries require some type of full-field measurement of displacements in order to determine strains. Digital image correlation (DIC) [27] is the most common choice and is used here, given its general ease of use and extensive development of analysis algorithms. In some cases, greater measurement resolution is required and so holography [28], moiré [18], speckle interferometry [29], and grid methods [30] have been used. Techniques with less spatial resolution than DIC include grip displacement [31] and marker tracking [32, 33].

Parameter identification from full-field heterogeneous strains is accomplished by the use of an inverse method. VFM [34] was chosen for this work because it is general, flexible, and faster than other methods which include FEM-Updating [25, 35], energy-based [36] and equilibrium gap [37] methods. VFM requires no additional programs, such as an FEM-solver, and analysis scripts can be easily written in Matlab®.

Ultrasonic techniques have also been used to determine the Q_{ij} of paper [38, 39]. Work by Habeger [39] appears to be the first attempt to determine Q_{16} and Q_{26} in paper materials. Three difficulties are associated with ultrasonic examination. First, significant wave attenuation occurs that requires sophisticated analysis to determine time-of-flight. Second, transmitted waves combine effects of all Q_{ij} and so relative scale of individual Q_{ij} makes it difficult to identify smaller parameters, such as Q_{16} and Q_{26}. Finally, in rate-dependent materials, ultrasonic properties depend on excitation frequency.

Two cellulose-fiber webs were examined: a filter paper and a paperboard, a packaging grade known in the industry as linerboard. Details of the load fixture and analysis method, along with quantification of parameter identification accuracy are provided. The VFM analysis was extended to include identification of Q_{16} and Q_{26}, along with associated methods to reduce effect of strain measurement noise. Whereas the analysis assumes that the materials are linear elastic and homogeneous, extension of the analysis to more general behavior is straight-forward. Comparison of Q_{ij} identification from VFM, ultrasonic and tensile coupons is included.

Material

Two materials were examined. The first material was Whatman® Chromatography Paper 3MM CHR and will be referred to as filter paper. It had nominal physical properties: grammage 180 g/m^2, thickness 0.28 mm, and density 635 kg/m^3. Filter papers are used in a variety of household, commercial, and scientific applications to capture particulate matter. The material was 100 % cellulose, as it is entirely comprised of cotton linters, a cellulose fiber that is typically 5–10 mm long.

The second material was a commercial unbleached, kraft single-ply linerboard that had nominal physical properties: grammage 209 g/m^2, thickness 0.30 mm, and density 688 kg/m^3. Fiber composition of this material is unknown, but likely contains both virgin and recycled fibers. This material is commonly used in structural products such as corrugated fiberboard containers. Even as nontraditional packaging is being developed more than 3.5B m^2 [40] corrugated sheet stock was produced in 2011.

The materials will be referred to as Filter and Linerboard, but such designation is not meant to indicate these materials are general representatives of filter papers and linerboards. Each of these materials can be manufactured with an almost endless variety of fiber furnish, drying, pressing, and additives.

Load Fixture

A schematic of the specially designed load fixture is shown in Fig. 1(a); the actual fixture is shown in Fig. 1(b). Forces are applied by four moveable grips on the top half of the fixture and measured with Sensotec (Honeywell International, Inc., Columbus, OH) Model 31BR load cells (range ±444 N) attached to Sensotec Model GM signal conditioners. The four grips located on the bottom half of the specimen are stationary. An additional fixture, not shown, was used as a template to cut the specimen and properly locate and punch holes for each grip. Prior to placing the specimen within the fixture, an alignment jig was used to adjust the top four grips to a precise starting location such that the specimen would experience no forces upon initial placement in the fixture. The aluminum knobs attached to the movable grips are rotated to generate radial tensile forces. A load configuration consisted of a unique force vector containing actual values for $F_1 - F_4$. Each specimen was subjected to multiple load configurations which created a series of different full-field strains for Q_{ij} evaluation. For each load configuration, individual forces were kept constant or increased, with respect to the previous load configuration, so that relaxation stiffnesses were avoided. As both materials were hygroscopic all tests were performed on the adsorption isotherm at 50 % RH, 23 °C.

The 24.5-cm-diameter specimen was gripped at eight locations 45° apart. Grips consisted of two small brass plates approximately 12 mm square. One plate had a threaded hole, the other a through-hole. Holes were punched at grip locations in the specimen, which was then clamped between plates with a small bolt. A torque wrench was used to ensure uniform clamping pressure for each grip. Special care was taken to prevent the top brass gripping plate from twisting and introducing undesirable stresses on the specimen. Without special care, the initial stress state around the grips would have compressive stresses on one side and tensile stresses on the other side.

Digital Image Correlation

We examined the surface of the paperboard with a Dantec® (Dantec Dynamics, Inc., Holtsville, NY) stereo DIC system whose details are listed in Table 1. An aluminum plate with a 9×9 grid of alternating black and white 11-mm squares was used for calibration. Calibration procedure located corners of the 11-mm squares to specify the global coordinate system and the intrinsic camera parameters, e.g., distortion and focal length. Fifteen calibration images were used for each calibration; a new calibration was performed each time a new specimen was placed in the load fixture. Appropriate facet size was determined by comparing the mean and standard deviation of strains calculated from a reference image and a no-load/no-displacement image and from a reference image and an image with a rigid body displacement. Both mean and standard deviation of ε_x and ε_y stabilized at a facet size of 21 pixels; larger facets continued to decrease strain standard deviation.

Displacements were smoothed by fitting a cubic spline to a 7×7 kernel of facets and replacing the center value with that determined by the cubic spline. Stiffness identification plateaued for smoothing kernel sizes between 5×5 and 9×9. Smaller kernels had erratic identification very sensitive to specific load configurations; as kernels became larger the strain gradients were smoothed to the extent that identification would not converge to optimum Q_{ij}. The 7×7 kernel was a good compromise that was insensitive to load configuration and had fast convergence.

The dot pattern was produced on the specimens using Sharp® (Sharp Electronics Corp., Mahwah, NJ) MX-3100 N copier. Static specimen images were captured by waiting 5 min after load configuration adjustment. A single reference image was used for each test. For each specimen, the initial load configuration had forces approximately 15 N greater, at each load grip, than forces for the reference image. Initial forces on the specimen were used to ensure that the specimen was planar and grips were fully engaged. A single image was used for each reference and deformed configuration. Images were not averaged because of the presence of some material nonlinearity.

The Virtual Fields Method

An abbreviated introduction to the VFM is presented in order to introduce extension of VFM to identify a fully populated Q_{ij} matrix; the recent book [34] provides full development of VFM. For a plane stress problem, the Principle of Virtual Work can be written as

$$\int_S \left(\sigma_1 \varepsilon_1^* + \sigma_2 \varepsilon_2^* + \sigma_6 \varepsilon_6^*\right) dS = \int_{L_f} \overline{T}_i u_i^* dl, \tag{1}$$

where S is the area of 2-D domain, σ_i are stresses within S, u_i^* are kinematically admissible virtual displacements, ε_i^* are virtual strains associated with u_i^*, $\overline{T}_i$ are tractions applied on boundary of S, and L_f is the portion of S over which $\overline{T}_i$ are applied.

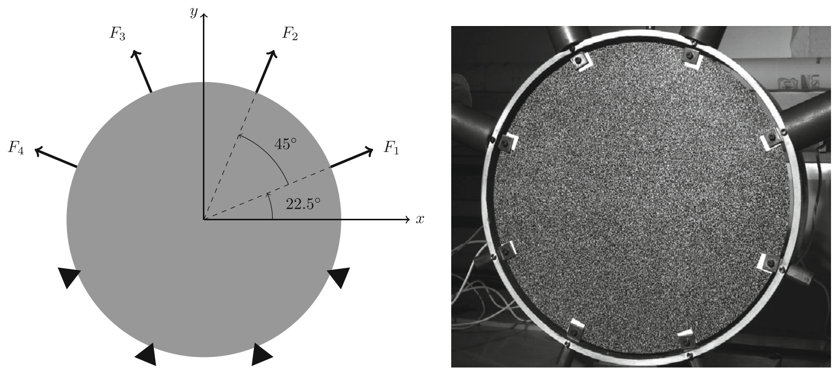

(a) Schematic of load fixture. (b) Actual load fixture as seen by one of the DIC cameras.

Fig. 1 Load fixture configuration. Diameter is 24.5 cm. White material near grips is reinforcing material

Assuming a linear elastic anisotropic material, the constitutive equation, using contracted index notation, is given by

$$\begin{Bmatrix} \sigma_1 \\ \sigma_2 \\ \sigma_6 \end{Bmatrix} = \begin{bmatrix} Q_{11} & Q_{12} & Q_{16} \\ Q_{12} & Q_{22} & Q_{26} \\ Q_{16} & Q_{26} & Q_{66} \end{bmatrix} \begin{Bmatrix} \varepsilon_1 \\ \varepsilon_2 \\ \varepsilon_6 \end{Bmatrix} \tag{2}$$

If the material is homogeneous, then each Q_{ij} is a constant and can be placed outside the integrals in Equation (1). Substituting Equation (2) into Equation (1) gives

$$\begin{aligned} &Q_{11} \int_S \varepsilon_1 \varepsilon_1^* dS + Q_{22} \int_S \varepsilon_2 \varepsilon_2^* dS + \cdots \\ &\cdots + Q_{12} \int_S \left(\varepsilon_1 \varepsilon_2^* + \varepsilon_2 \varepsilon_1^*\right) dS + \cdots \\ &\cdots + Q_{16} \int_S \left(\varepsilon_1 \varepsilon_6^* + \varepsilon_6 \varepsilon_1^*\right) dS + \cdots \\ &\cdots + Q_{26} \int_S \left(\varepsilon_2 \varepsilon_6^* + \varepsilon_6 \varepsilon_2^*\right) dS + \cdots \\ &\cdots + Q_{66} \int_S \varepsilon_6 \varepsilon_6^* dS = \int_{L_f} \overline{T}_i u_i^* dl \end{aligned} \tag{3}$$

Table 1 DIC system components and parameters

Camera	Allied Vision Technologies (Stadtroda, Germany) Stingray Model F504B
Lens	Computar (Commack, NY) M1614-MP2, 16 mm, f1.4
Lighting	Red LED, 4×3 array, wavelength 610–640 nm
Resolution	2452×2056
Facet size	21 pixels, approx 3.3 mm×3.3 mm
Software	Istra (Dantec) 4-D v2.1.5
Displacement smoothing	7×7 kernel of facets
Strain calculation	Central finite difference

In practice, six different u_i^* are used in Equation (3), one to identify each Q_{ij}. Special virtual fields simplify identification by choosing six different u_i^* so that only one integral term, one for each Q_{ij}, exists on the left side of Equation (3). Special virtual fields are thoroughly discussed in [34]. Their use greatly simplifies programming and solution. Consider the special virtual field used to identify Q_{11}, which is denoted by $u_i^{*(1)}$, where (1) is associated with Q_{11}. $u_i^{*(1)}$ is called a special virtual field if all the other integral terms sum to 0 and the integral term associated with Q_{11} sums to 1. Using this field, Equation (3) becomes

$$Q_{11} \int_S \varepsilon_1 \varepsilon_1^{*(1)} dS = Q_{11} = \int_{L_f} \overline{T}_i u_i^{*(1)} dl \tag{4}$$

By creating a special virtual field for each Q_{ij} the determination for each Q, in the absence of measurement noise, becomes trivial.

By approximating the integrals in Equation (3) as discrete summations, a system of linear equations is developed whose solution requires minimal computation. As described earlier, DIC provides information on each ε_i throughout specimen surface and load cells provide values for each $\overline{T}_i$.

An important part of VFM analysis is to characterize the sensitivity of the identified parameters to strain noise. This work extends VFM to reduce the sensitivity to noise on parameter identification of Q_{16} and Q_{26} using the same procedure given by Avril et al. [41] for orthotropic Q_{ij}. They showed that variance of each Q_{ij}, $\mathbf{V}(\mathbf{Q})$, due to noise in strain measurements was given by

$$\mathbf{V}(\mathbf{Q}) = \gamma^2 \left(\frac{S}{n}\right)^2 \mathbf{Q}^{\mathbf{app}} \cdot \mathbf{G} \cdot \mathbf{Q}^{\mathbf{app}}, \tag{4}$$

where γ is the amplitude of the strain noise represented by a zero-mean Gaussian distribution, S is the area of the specimen, n is the number of discrete measurements within S, $\mathbf{Q}^{\mathbf{app}}$ is the approximate Q_{ij} assuming noise is present but not accounted for and the non-zero terms of **G** are the following:

$$G(1,1) = \sum_{i=1}^{n} \left(\varepsilon_{1,k}^{*(ij)}\right)^2 \tag{5}$$

$$G(1,3) = G(3,1) = \sum_{i=1}^{n} \varepsilon_{1,k}^{*(ij)}\varepsilon_{2,k}^{*(ij)}$$

$$G(1,5) = G(5,1) = \sum_{i=1}^{n} \varepsilon_{1,k}^{*(ij)}\varepsilon_{6,k}^{*(ij)}$$

$$G(2,2) = \sum_{i=1}^{n} \left(\varepsilon_{2,k}^{*(ij)}\right)^2$$

$$G(2,3) = G(3,2) = \sum_{i=1}^{n} \varepsilon_{1,k}^{*(ij)}\varepsilon_{2,k}^{*(ij)}$$

$$G(2,6) = G(6,2) = \sum_{i=1}^{n} \varepsilon_{2,k}^{*(ij)}\varepsilon_{6,k}^{*(ij)}$$

$$G(3,3) = \sum_{i=1}^{n} \left(\varepsilon_{1,k}^{*(ij)}\right)^2 + \sum_{i=1}^{n} \left(\varepsilon_{2,k}^{*(ij)}\right)^2$$

$$G(3,5) = G(5,3) = \sum_{i=1}^{n} \varepsilon_{2,k}^{*(ij)}\varepsilon_{6,k}^{*(ij)}$$

$$G(3,6) = G(6,3) = \sum_{i=1}^{n} \varepsilon_{1,k}^{*(ij)}\varepsilon_{6,k}^{*(ij)}$$

$$G(4,4) = \sum_{i=1}^{n} \left(\varepsilon_{6,6}^{*(ij)}\right)^2$$

$$G(4,5) = G(5,4) = \sum_{i=1}^{n} \varepsilon_{1,k}^{*(ij)}\varepsilon_{6,k}^{*(ij)}$$

$$G(4,6) = G(6,4) = \sum_{i=1}^{n} \varepsilon_{2,k}^{*(ij)}\varepsilon_{6,k}^{*(ij)}$$

$$G(5,5) = \sum_{i=1}^{n} \left(\varepsilon_{1,k}^{*(ij)}\right)^2 + \sum_{i=1}^{n} \left(\varepsilon_{6,k}^{*(ij)}\right)^2$$

$$G(5,6) = G(6,5) = \sum_{i=1}^{n} \varepsilon_{1,k}^{*(ij)}\varepsilon_{2,k}^{*(ij)}$$

$$G(6,6) = \sum_{i=1}^{n} \left(\varepsilon_{2,k}^{*(ij)}\right)^2 + \sum_{i=1}^{n} \left(\varepsilon_{6,k}^{*(ij)}\right)^2$$

where $\varepsilon_{m,k}^{*(ij)}$ is the special virtual strain (m=1,2 or 6) for the discrete region, k, associated with identification of a particular stiffness Q_{ij}.

Defining

$$\mathbf{V}(\mathbf{Q}) = \gamma^2\eta^2 \tag{6}$$

the standard deviations of Q_{ij} are given by η_{ij}. Because of the great differences in magnitude of Q_{ij} the coefficients of variation, η_{ij}/Q_{ij}, are commonly used to compare sensitivity of identified Q_{ij} to strain noise.

The remainder of the description regarding the use of **G** to minimize the effect of measurement noise on the identification of Q_{ij} corresponds to that given by Pierron and Grédiac [34], except that some scaling was used to reduce effects of great differences in magnitude of Q_{ij}. The larger **G** (6×6 for anisotropy vs 4×4 for orthotropy) given in Equation (5) slightly increases the number of iterations used for identification. In this work six iterations were typically sufficient for identification.

Selection of VFM Mesh

Most VFM applications use a virtual mesh of 4-node quadrilateral isoparametric elements, similar to a FEM mesh, to create kinematically admissible virtual fields. However, VFM mesh density analysis has no analogy to FEM mesh convergence studies, but balances competing influences of sufficient degrees of freedom for accurate parameter identification with the knowledge that increased mesh density amplifies the effects of strain noise and decreases accuracy of identification. Figure 2(a–c) show example VFM meshes at three mesh densities.

Choice of VFM mesh density for subsequent parameter identification was based on mesh's capacity to identify Q_{12} as the smallest Q_{ij} that was sure to exist; both Q_{16} and Q_{26} may be zero. Effect of mesh density on Q_{12} identification is shown in Fig. 3; units are km^2/s^2, or specific stiffness units, and are equivalent to MN·m/kg. Selection of load configurations used to identify Q_{12} in Fig. 3 are discussed in the Analysis section and were confined to those in the linear elastic regime.

The criteria for mesh density was to choose the coarsest mesh that had sufficient degrees of freedom to identify all Q_{ij} and was appropriate for both materials. The difficulty for a 25-element mesh to identify small Q_{12} is not surprising as the mesh contains only four interior, unconstrained nodes, and therefore eight degrees of freedom, to identify six Q_{ij}. Above 225 elements Q_{12} the ability to detect small Q_{12} tends to decrease. The 36-element mesh appeared to have difficulty discerning the Poisson effect, probably because of interior node locations that experienced very low strains. The 49-element mesh, Fig. 2(b), contains 24 interior, unconstrained nodes and appeared to be the coarsest mesh, to reduce the effects of strain noise, for good identification and was used for all subsequent analyses. Differences in Q_{12} identification between the 49- and 64-element meshes were small and so the coarser mesh was selected.

In order to have a kinematically admissible virtual field, grip nodes are virtually fixed in both u and v displacement because they correspond to stationary grips in Fig. 1(a). Additionally, radially oriented forces are prescribed at the load grips corresponding to forces F_4,

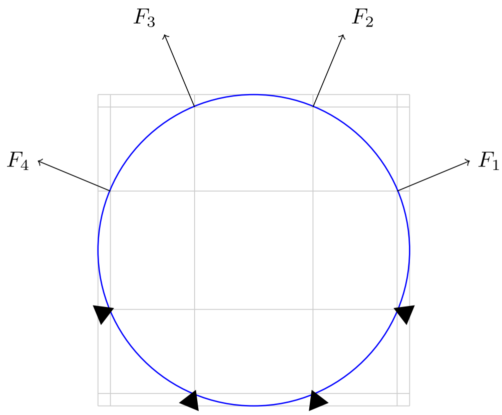

(a) Example of 25 element virtual mesh.

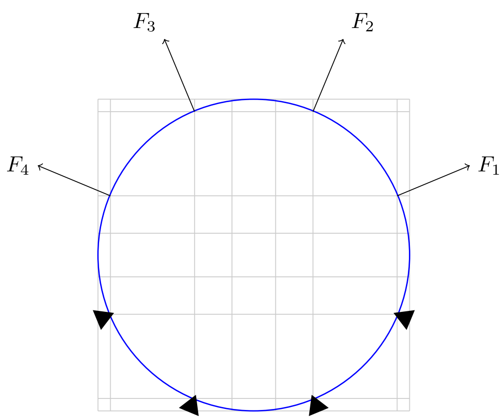

(b) Example of 49 element virtual mesh.

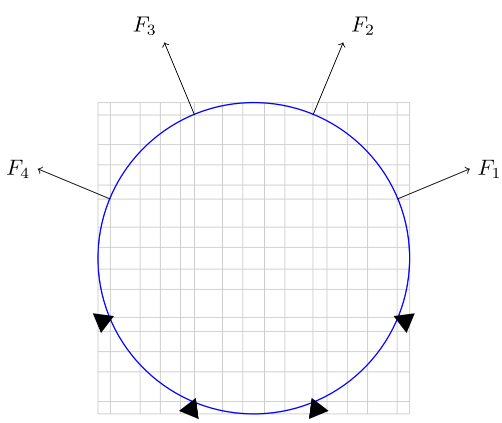

(c) Example of 225 element virtual mesh.

Fig. 2 Examples of different VF meshes for geometry in Fig. 1(a). Meshes are required to have nodes at each force and fixed grip

F_3, F_2, and F_1. VFM meshes are not required to conform to specimen boundaries. Some VFM elements lie completely outside the specimen area, S, while other elements straddle the external boundary of S. Only terms in Equation (3) with nonzero, experimentally measured ε_i have a contribution to stiffness evaluation.

Supporting Tests

Ultrasonic tests on individual specimens were performed with a Nomura Shoji® SST-250 paper tester. Transmission probe oscillated at 25 kHz. A central circular region, with 15-cm diameter, was examined for each specimen. Ultrasonic velocity was measured from 0 to 175 ° in 5 ° increments. Q_{66} was determined by measuring shear wave velocity transmitted along the 2-principal material direction using a second, modified SST instrument. The Musgrave Transformation [42, 43] was used to convert from wave velocity to phase velocity. Phase velocity was used to determine remaining stiffnesses, as Q_{66} was determined directly, according to the procedure described by Habeger [39].

Anisotropic stiffness transformation, Equation (7), was used to fit the ultrasonic phase velocity data, $Q_{11}^{'}$.

$$Q_{11}^{'} = Q_{11}cos^4\theta + 2(Q_{12} + 2Q_{66})cos^2\theta sin^2\theta + Q_{22}sin^4\theta - \cdots \\ \cdots - 4Q_{16}cos^3\theta sin\theta - 4Q_{26}cos\theta sin^3\theta \tag{7}$$

Three tensile coupons were cut from each circular specimen after DIC and ultrasonic evaluations. Coupons were cut at 0 °, 45 °, 90 ° from 1-principal material direction. Coupons were 25 mm wide and each had a nominal gage length of 175 mm. Specimens were tested in an Instron® Model 5865 load frame with a grip displacement rate of 0.5 mm/min. DIC images were captured at 1 Hz and used to determine longitudinal and transverse strains. Longitudinal strains were used to determine E_{11} and E_{22} and transverse strains were used to determine ν_{12} and ν_{21} using the 0° and 90° coupons, respectively. Q_{66} was determined using data from all three coupons by stiffness transformation (equation (8)), as described in several sources, e.g., Jones [44].

$$Q_{66} = \frac{1}{\left(\frac{4}{E_{45}} - \frac{1}{E_{11}} - \frac{1}{E_{22}} + \frac{2\nu_{12}}{E_{11}}\right)} \tag{8}$$

Each test, VFM, ultrasonic and tensile, identifies a different Q_{ij}; VFM identifies secant tensile stiffness, ultrasonic identifies compression stiffness at very low strain levels and tensile identifies tangent tensile stiffness. For a linear elastic material all these different types of stiffness are the same. For nonlinear, viscoelastic materials ultrasonic Q_{ij} will be greater than the VFM secant Q_{ij}, that will, in turn, be greater than tensile Q_{ij}.

The rationale for choosing tangent stiffness as opposed to secant stiffness for tensile data was made because selection of the appropriate applied force to compare with this new geometry is not possible and tangent stiffness is used throughout the paper industry. The choice to use secant stiffness as opposed to tangent stiffness for this new geometry was based on the difficulty to measure strains between two adjacent load increments; importance of developing sufficient strains for Q_{ij} identification will be discussed in the next section.

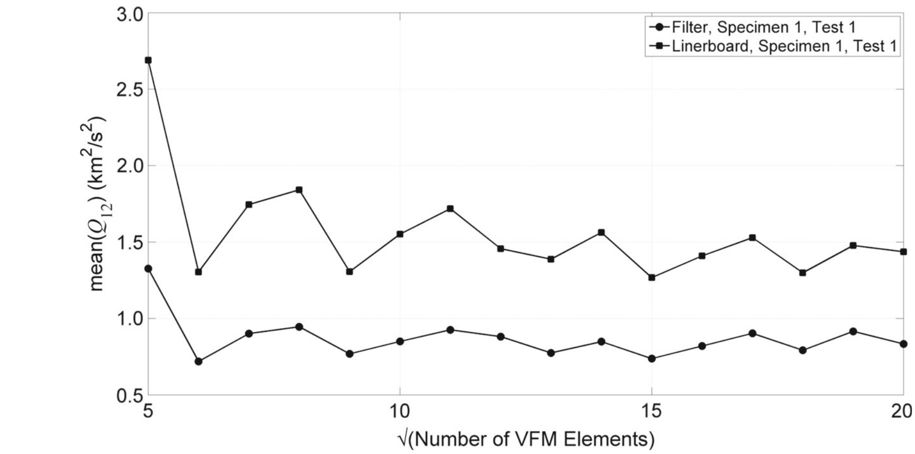

Fig. 3 Q_{12} identification for different VFM mesh densities

Analysis

Three different specimens for each material, filter, and linerboard were tested with a minimum of 10 load configurations; after the initial test, specimens were removed from load fixture, reinserted, and retested.

As both materials were known to have nonlinear behavior, it was assumed that only a range of load configurations could be used for linear elastic parameter identification. Determination of material nonlinear behavior is not straightforward for this load fixture. As the geometry was intentionally designed to produce sufficient strains, ε_i, for evaluation of all six Q_{ij}, it is not possible to directly determine onset of material nonlinear behavior. Furthermore, nonlinear behavior is unlikely to occur simultaneously for each Q_{ij}. An example pair of tests for each material is shown in Fig. 4, which examines the manner in which forces induced strain in these tests, where norm refers to 2-norm, ε_c is given by Equation (9) and n is the number of strain measurements on the specimen surface. This figure suggests that the specimens behaved elastically for each load configuration and for each test. Elastic behavior is illustrated by the relative coincidence of points for each test of each material.

$$\varepsilon_c = \frac{1}{3n}\sqrt{\sum_{i=1}^{n}\left[\left(\varepsilon_{1,i}\right)^2 + \left(\varepsilon_{2,i}\right)^2 + \left(\varepsilon_{6,i}\right)^2\right]} \tag{9}$$

Figure 4 indicates nonlinear behavior occurred for both materials, but does not indicate non-linearity occurred for all ε_i and at all locations within the specimen. Nonlinear behavior was more likely to occur near the eight grips. Based on similar behavior for repeated tests, parameter identification was limited to load configurations where norm (F_i) was less than 65 N for Filter and 80 N for Linerboard.

An additional tool to determine quality of parameter identification is the comparison of η_{ij}/Q_{ij} for each load configuration, as seen in Figs. 5 and 6; η_{16}/Q_{16} and η_{26}/Q_{26} are not shown to reduce vertical scale. Strains used for identification were determined from a single reference image, one for each material. Applied forces were the difference between those in the analyzed image and the reference image. Horizontal axes in these figures corresponds to vertical axis in Fig. 4. An incremental analysis, where two consecutive loadings are

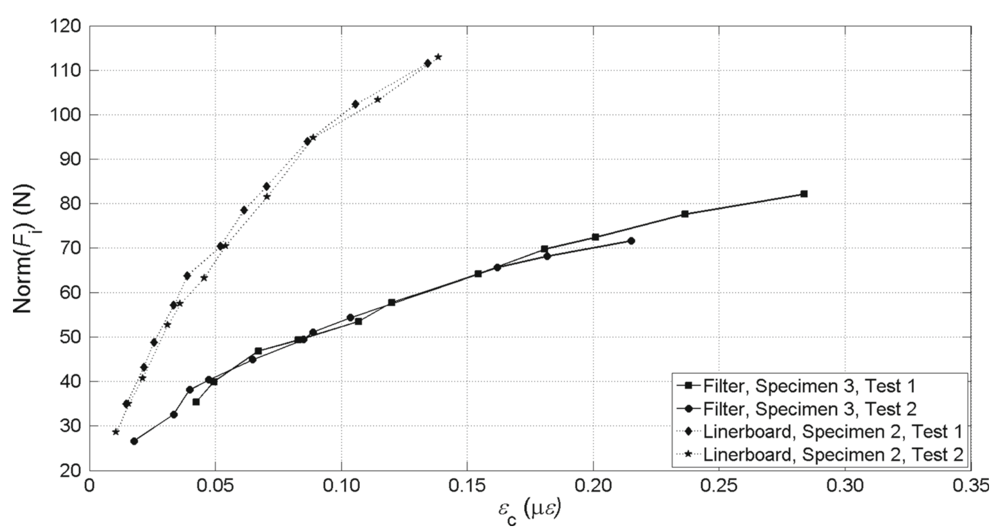

Fig. 4 Examination of applied forces and induced strain for Filter, Specimen 3 and Linerboard, Specimen 2, where ε_c is given by Equation 9

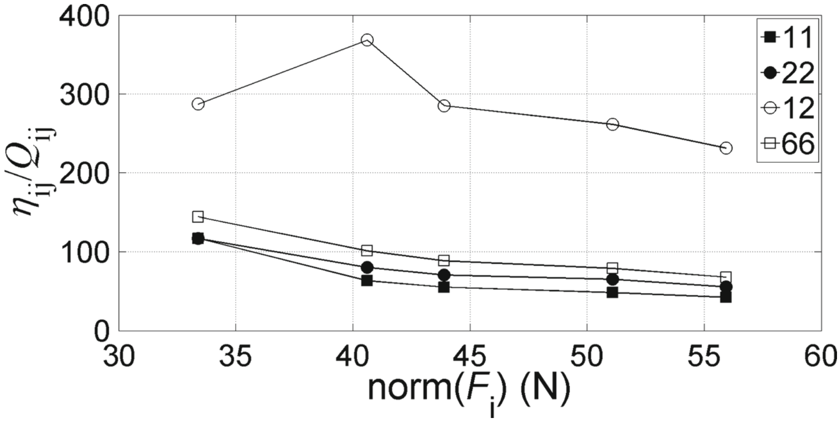

Fig. 5 COV for Filter, Specimen 2, Test 2

compared, was not used because strain differences between two consecutive loadings were too small for identification. As expected, η_{12}/Q_{12} was higher than other η_{ij}/Q_{ij} because Q_{12} is generally smaller than Q_{11}, Q_{22}, and Q_{66} and is more difficult to identify as demonstrated by the non-monotonic behavior of η_{12}/Q_{12} with increasing norm (F_i). The other η_{ij}/Q_{ij} behaved consistently with improved identification, i.e. lower η_{ij}/Q_{ij}, with increasing forces and strains. Figures 5 and 6 were representative of identifications for each material. Based on this analysis, load configurations with any of η_{11}/Q_{11}, η_{22}/Q_{22}, or η_{66}/Q_{66} above 100 for Filter and above 200 for Linerboard were not used for identification.

High η_{ij}/Q_{ij} for load configurations where norm (F_i) is less than 40 N, for either material, was expected given resolution of DIC strains. Figure 7 shows DIC strain for three scenarios, 7(a–c), that had no change in forces between reference and analyzed image so norm (F_i)=0 N, 7(d–f) Linerboard, Specimen 1, Test 1, Load Configuration 1, where norm(F_i)= 34 N and, 7(d–f) Linerboard, Specimen 1, Test 1, Load Configuration 5, where norm(F_i) =62 N. (Load configurations for each material and test are given in the Appendix in Tables 3 and 4. The last column identifies those configurations used in identification.) Strain contours for 7(a) through 7(f) have few obvious differences while strain gradients for 7(g–i) are more apparent. Furthermore, differences between the Q_{11}, Q_{22}, Q_{12}, and Q_{66} comparing 7(d–f) to 7(g–i) were only 13.8 %, −5.9 %, −13.3 % and −6.2 %, respectively, and validate the performance of VFM. The standard deviations in Fig. 7 captions are for the entire specimen and demonstrate the ability of VFM to identify stiffnesses even when only small regions of the specimen, e.g., near the grips, have significant strains. The standard deviation of strains for the no load and Load Configuration 1 were very similar, showing that Load Configuration 1 had strain only slightly above the strain noise. The scale used in Fig. 7 is quite small, hence the difficulty with identification. So, while parameter identification seemed reasonable for small norm (F_i), those individual load configurations with high η_{ij}/Q_{ij}, as discussed earlier, were not used in the final analyses.

Results and Discussion

After selection of load configurations for each test, those load configurations were superimposed to create a single, superposition load condition where ε_1, ε_2, and ε_6 were created by the

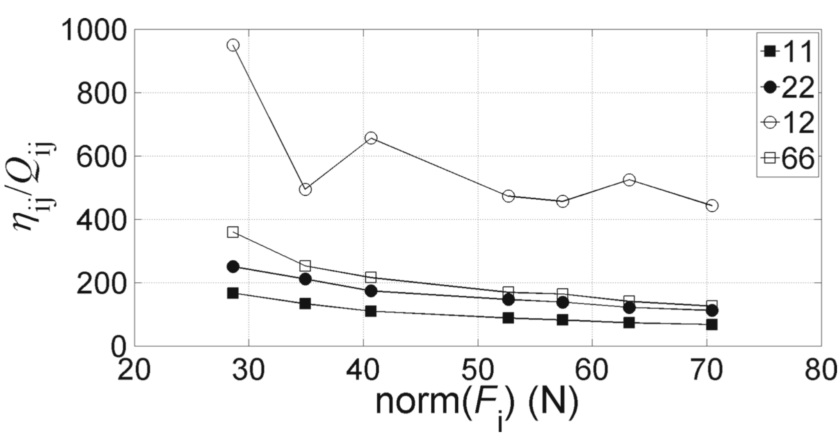

Fig. 6 COV for Linerboard, Specimen 2, Test 2

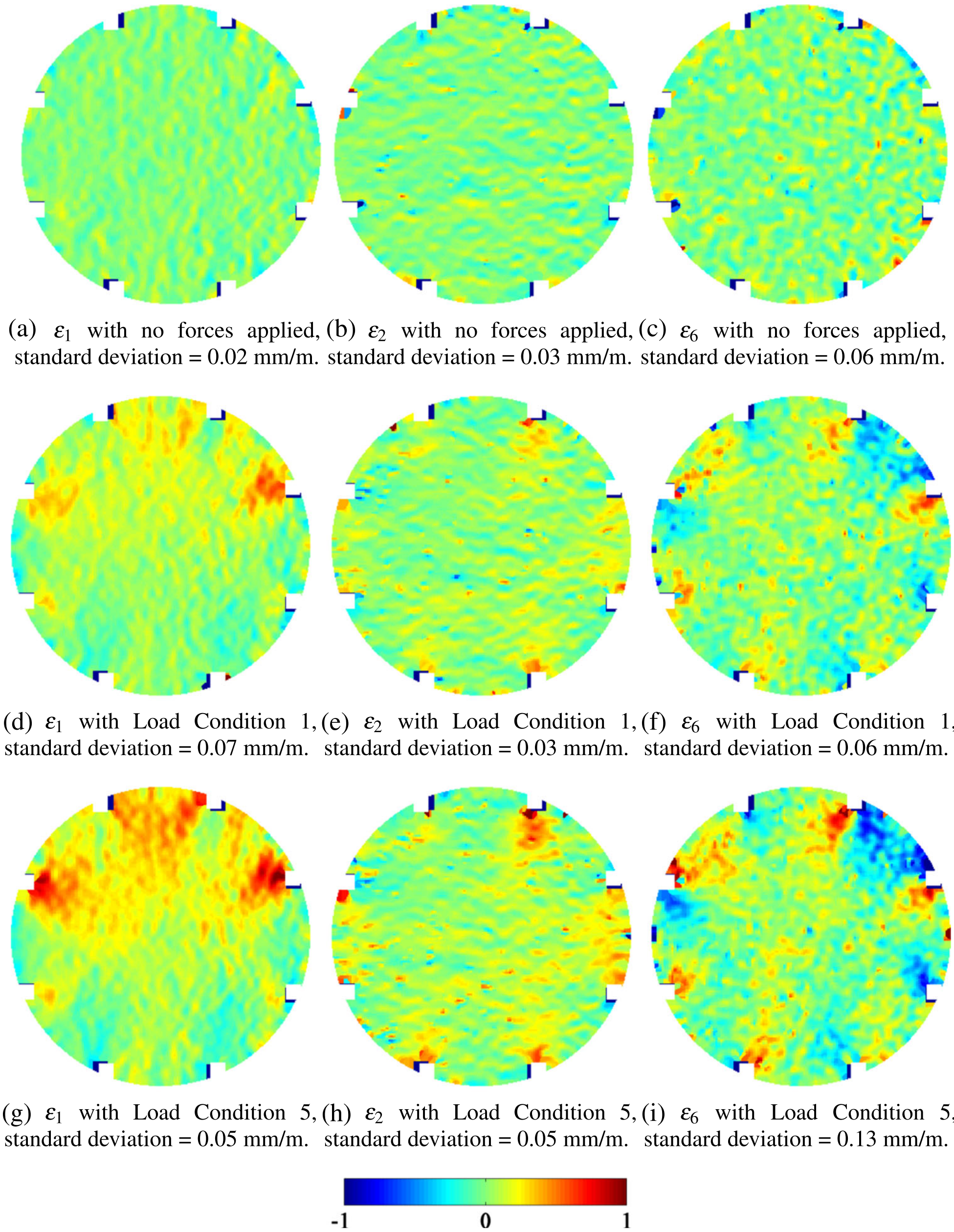

(a) ε_1 with no forces applied, standard deviation = 0.02 mm/m. (b) ε_2 with no forces applied, standard deviation = 0.03 mm/m. (c) ε_6 with no forces applied, standard deviation = 0.06 mm/m.

(d) ε_1 with Load Condition 1, standard deviation = 0.07 mm/m. (e) ε_2 with Load Condition 1, standard deviation = 0.03 mm/m. (f) ε_6 with Load Condition 1, standard deviation = 0.06 mm/m.

(g) ε_1 with Load Condition 5, standard deviation = 0.05 mm/m. (h) ε_2 with Load Condition 5, standard deviation = 0.05 mm/m. (i) ε_6 with Load Condition 5, standard deviation = 0.13 mm/m.

Fig. 7 DIC strains for (**a**–**c**) no applied forces, (**d**–**f**) Linerboard, Specimen 1, Test 1, Load Configuration 1 (**g**–**i**) Linerboard, Specimen 1, Test 1, Load Configuration 5; units for scale (mm/m). Specimen diameter=24.5 cm

addition of the ε_i from each load condition and the F_i were created by the addition of forces from each load condition. A minimum of three load conditions were combined for each superposition identification. From Fig. 7, it is apparent that the specimen regions near the grips provided the necessary strain intensity for identification. Different load conditions changed regions of intensity and gradients, while superposition of the selected load conditions provided gradient-rich strain maps improving identification. The manner in which grip regions affected identification and critical area of specimen needed for identification were not studied here. An ancillary numerical study showed good stiffness identification on regions as small as 7 % of total specimen area even when the smaller region was located near center of the specimen.

Figure 8 shows those results along with Q_{ij} determined from ultrasonic and tensile tests. (Appendix Table 5 lists the results used to make these plots.) Equation 7, the anisotropic stiffness transformation for Q_{11}, was used to make the plots in Fig. 8.

Table 2 give the anisotropic stiffness invariants, I_1 and I_2, as determined by [45] and are given in Equation (10). These invariants were chosen because they are independent of z-direction symmetry. Other invariants may exist; these were selected as an example to determine robustness of the load fixture and VF analysis. The last column, ϕ, represents the

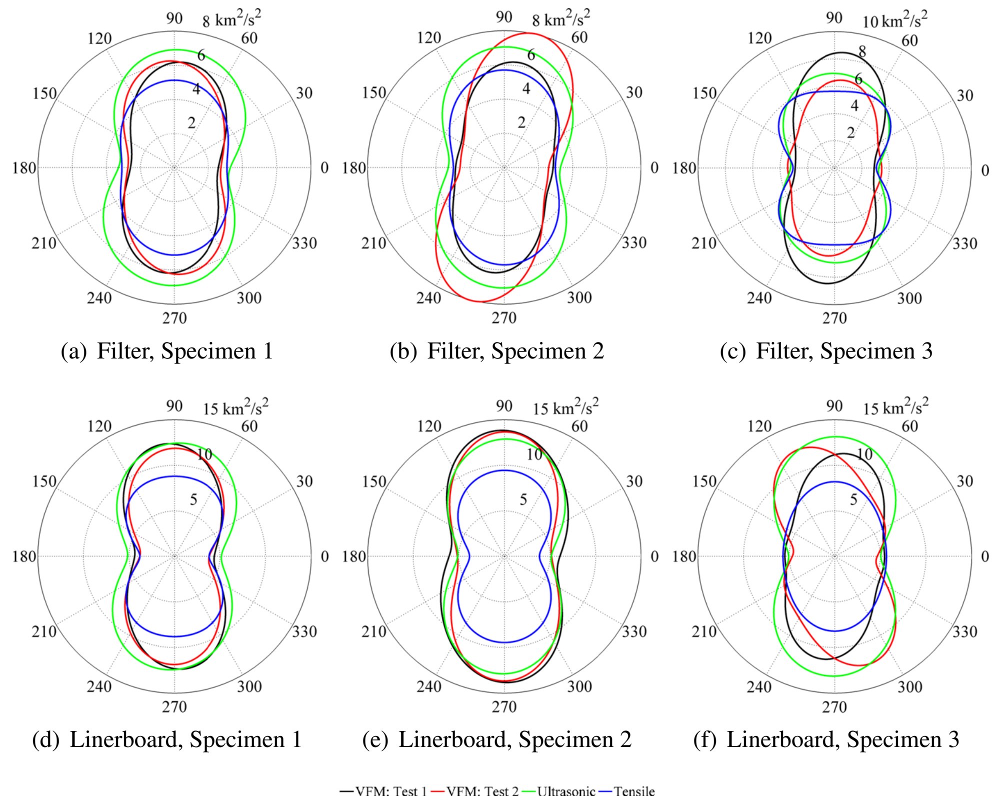

Fig. 8 Polar plot of Q_{11} for each of the six specimens, stiffness units are km^2/s^2, angle units are degrees

difference from orthotropy as determined from Equation (12) from [39] where $\phi=0^\circ$ would be a perfectly orthotropic material and $\phi=10^\circ$ would denote an anisotropic material whose 1- and 2-principal material directions, where 1- and 2-direction correspond directions of maximum Q_{11} and Q_{22}, respectively, are oriented 80° to each other.

$$\begin{aligned} I_1 &= Q_{11} + Q_{22} + 2Q_{12} \\ I_2 &= Q_{66} - Q_{12} \end{aligned} \tag{10}$$

$$\phi = -\frac{Q_{16}}{Q_{11} - Q_{12} - 2Q_{66}} - \frac{Q_{26}}{Q_{22} - Q_{12} - 2Q_{66}} \tag{11}$$

The 1-principal direction was nearly vertical (y-axis in Fig. 1(a)) for all tests so $Q_{22}>Q_{11}$; this specimen orientation was intentionally used to develop more strain in the stiffest direction because the y-axis is bracketed by load grips while the x-axis is bracketed by a load and stationary grip. Load fixture and circular specimen shape suggested three additional tests could be performed on the same specimen by $\pi/4$ rotations. These additional tests gave gave similar results, but are not reported here for brevity.

VFM identified Q_{11} and Q_{22} were generally larger than those determined by tensile tests and smaller than those identified ultrasonically and suggests that some nonlinear behavior was present. Ultrasonic identification of Q_{12} is difficult, because Q_{66} and Q_{12} are coupled, as given in Equation (7), and so errors in Q_{66} are propagated to Q_{12} and that Q_{12} has a smaller contribution to the phase velocity than Q_{11} and Q_{22}. Comparison of the invariants, I_1 and I_2, shows good agreement between VFM and tensile values while individual specimen ultrasonic values were higher for I_1 and lower for I_2.

Filter had general agreement with Q_{11} and Q_{22} among the tests, while Q_{12} and Q_{66} were lower for VFM identification than for ultrasonic or tensile tests. For an orthotropic material Q_{12} is the most difficult to identify using inverse methods [34]. However the consistently lower values for Q_{12} and the general agreement of the invariants suggest that the secant Q_{12} may be lower than Q_{12} identified with other methods. Differences between identification methods were more apparent for Linerboard. Q_{11} and Q_{22} were comparable for VFM and ultrasonic tests and were higher than for tensile tests. Those results agree with differences between secant and tangent modulus for nonlinear materials. As with Filter, the invariants of VFM and tensile were more similar than for ultrasonic tests. In general, the pattern of differences between Q_{ij} from each identification method were expected given that both materials have nonlinear behavior and sufficient strain is required to provide reasonable identification.

The combination of Q_{16}, Q_{26} and ϕ values near zero suggest that both materials were orthotropic. Linerboard, Specimen 3, Test 2 demonstrates rotated orthotropy because it had non-zero shear-coupled stiffnesses but near zero ϕ value. This particular test indicated the specimen was rotated

Table 2 Invariants and anisotropy angle, ϕ for each specimen and test. Units for I_1 and I_2 are km^2/s^2; units for ϕ are degrees

Material	Specimen	Test	I_1	I_2	ϕ
Filter	1	VFM-Test1	10.6	0.4	−0.04
		VFM-Test2	10.5	0.8	−0.14
		Ultrasonic	14.6	−0.5	−0.09
		Tensile	10.8	0.2	N/A
	2	VFM-Test1	10.5	0.4	−0.12
		VFM-Test2	12.2	0.3	0.23
		Ultrasonic	14.5	−0.4	−0.06
		Tensile	11.4	0.3	N/A
	3	VFM-Test1	13.5	0.3	0.04
		VFM-Test2	12.1	0.0	−0.05
		Ultrasonic	14.9	−0.7	−0.08
		Tensile	11.3	1.5	N/A
Linerboard	1	VFM-Test1	20.2	0.8	−0.13
		VFM-Test2	18.5	1.3	−0.07
		Ultrasonic	26.8	−2.1	0.05
		Tensile	15.4	2.2	N/A
	2	VFM-Test1	24.2	1.1	−0.22
		VFM-Test2	22.6	0.8	0.08
		Ultrasonic	26.3	−1.7	−0.02
		Tensile	16.3	1.6	N/A
	3	VFM-Test1	19.4	0.7	0.26
		VFM-Test2	18.8	2.0	−0.74
		Ultrasonic	27.5	−2.2	0.03
		Tensile	17.7	0.3	N/A

7.4 ° within the load fixture. Using stiffness transformation, the values for Q_{22}, Q_{11}, Q_{12}, and Q_{66} are 11.32, 5.61, 0.95, and 2.97 respectively, and have better agreement with Q_{ij} associated with Test 1 of that specimen.

Test repetition was used to demonstrate repeatability of results. As shown in Fig. 4, applied forces produced similar strains for the first and second tests of each specimen. Appendix Table 5 show good repeatability of Q_{ij} for each replication. Differences can be justified by a small specimen rotation disagreement between tests, as discussed previously, or by some specimen damage caused by unintentional plastic deformation. Specifically, damage seems to have occurred during tests of Linerboard, Specimens 1 and 2 because Q_{ij} for Test 1 were higher than for Test 2.

Parameter identification by inverse methods is improved by using the experimentally measured data to determine the fewest possible parameters. As our identification results indicate both materials were orthotropic, it is appropriate to examine the possibility that the materials were 'special' orthotropic in which Q_{66} is independent of orientation angle, as most recently discussed by Ostoja-Starzewski and Stahl [46] and predicted for other composite materials by Vannucci [47]. For materials of this type, the normal four orthotropic constitutive parameters are reduced to three according to Equation (12), where E_{11}, E_{22}, ν_{12}, and ν_{21} can be expressed in terms of Q_{11}, Q_{22}, and Q_{12}. Figure 9 compares the identified Q_{66} with Q^s_{66} as determined by Equation (12), where those parameters were determined by rotating the VFM-identified Q_{ij} to their principal directions. Figure 9 suggests that Filter and Linerboard may be special orthotropic, but additional testing would be required for more definitive affirmation.

$$\frac{1}{Q^s_{66}} = \frac{1+\nu_{12}}{E_{11}} + \frac{1+\nu_{21}}{E_{22}} \quad (12)$$

Conclusion

A new load fixture and VFM parameter identification process applicable to general anisotropic sheet materials have been created. This process improves parameter identification in cases where material principal directions are not known a priori or specimen fabrication is not aligned with material principal directions.

An overview was presented of the manner in which this new load fixture can be used for parameter identification. Future use of this fixture will quantify the effect of specimen orientation and load configuration on identified parameters, similar to that performed by Pierron et al. [48] and Rossi and Pierron [49] on the unnotched Iosipescu specimen geometry. Some combination of orientation and load configuration may

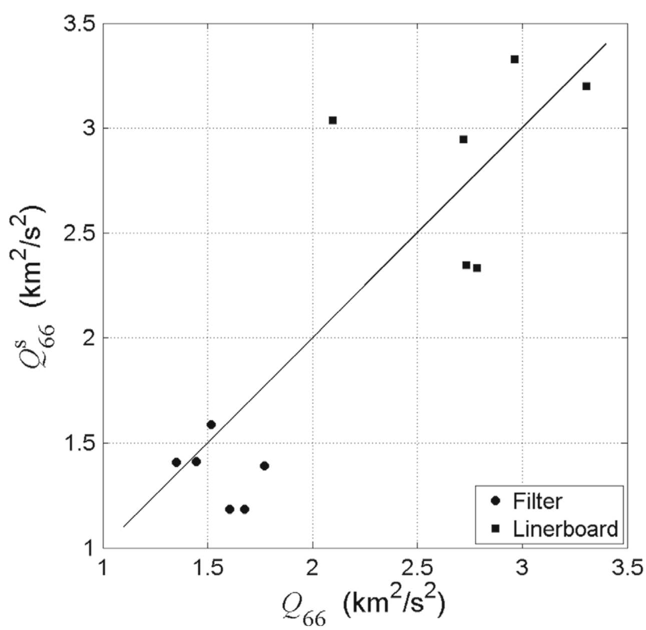

Fig. 9 Examination of angular independence of Q_{66}; line denotes Q_{66}= Q^s_{66} and is not a fit to the data

provide optimum strain contours to improve identification and reduce noise effects.

This work extended VFM identification to general anisotropic sheet materials and introduced a novel load fixture designed to produce the necessary strain fields. DIC was used to investigate full-field strains under a variety of multi-axial load configurations for two different paper materials. Quantification of nonlinear constitutive behavior, quality of parameter identification, and examination of the effect of VFM mesh density were performed. For each material, VFM-evaluated Q_{ij} were repeatable and compared favorably with those determined by ultrasonic and tensile coupon tests. A multi-step process is provided to improve VFM parameter identification through recognition of orthotropy and to recognize independence of angular orientation of Q_{66}.

Appendix

Appendix Tables 3 and 4 give the load configurations for each test. The last column indicates tests used for identification.

Identified Q_{ij} for each test and were used to create Fig. 8.

Table 3 Load configurations for Filter, units (N)

Specimen	VFM test	Load configuration	F_1	F_2	F_3	F_4	Norm(F_i)	Used for identification
1	1	1	16.90	17.35	18.99	17.79	35.55	
		2	18.24	21.35	27.49	19.13	43.70	
		3	19.13	22.69	27.62	20.91	45.61	*
		4	21.80	26.69	29.49	22.24	50.52	*
		5	24.02	30.69	32.69	25.35	56.84	*
		6	25.80	35.59	38.48	30.69	65.99	
		7	28.47	37.37	39.06	32.03	68.98	
		8	29.80	38.25	40.03	33.36	71.19	
		9	33.36	42.26	45.33	37.37	79.68	
		10	35.14	44.04	47.51	40.03	83.87	
	2	1	17.79	16.01	17.88	15.57	33.69	
		2	17.35	20.02	21.31	14.68	37.03	
		3	18.24	22.69	24.29	17.35	41.69	
		4	20.46	26.69	27.76	20.02	47.98	*
		5	23.13	28.91	29.71	21.80	52.24	*
		6	25.35	30.69	31.36	21.80	55.17	*
		7	26.69	34.70	35.81	23.58	61.27	*
		8	29.36	36.48	37.90	25.35	65.36	
		9	32.03	38.25	41.46	28.47	70.84	
		10	36.92	44.04	44.30	33.81	80.05	
2	1	1	14.23	16.90	21.97	12.01	33.40	
		2	16.01	21.35	25.53	16.90	40.62	
		3	17.79	21.35	28.38	18.68	43.90	
		4	23.58	25.35	30.29	22.24	51.10	*
		5	25.80	29.36	31.67	24.47	55.94	*
		6	28.47	32.47	34.70	26.24	61.30	*
		7	30.25	33.36	36.43	27.58	64.15	*
		8	32.47	35.14	40.17	29.80	69.22	
		9	33.81	36.92	40.92	30.69	71.57	
		10	33.81	40.03	43.33	33.81	75.93	
		11	34.70	44.04	45.55	37.81	81.53	

Table 3 (continued)

Specimen	VFM test	Load configuration	F_1	F_2	F_3	F_4	Norm(F_i)	Used for identification
3	2	1	12.90	21.35	19.53	17.35	36.12	
		2	15.12	24.02	23.00	20.02	41.66	
		3	16.46	25.35	25.93	24.02	46.51	
		4	17.79	27.13	27.85	27.13	50.64	*
		5	19.57	29.36	30.25	28.47	54.50	*
		6	20.91	32.47	33.14	31.14	59.66	*
		7	23.13	34.70	35.50	32.47	63.67	*
		8	24.47	36.48	37.01	34.25	66.87	
		9	28.02	38.25	38.61	36.03	70.98	
		10	29.36	38.70	40.83	38.70	74.33	
		11	32.47	42.70	47.91	40.03	82.32	
	1	1	16.90	20.02	17.13	16.46	35.36	
		2	18.24	22.24	21.57	17.35	39.92	
		3	21.80	26.24	24.78	20.46	46.87	
		4	22.69	28.02	25.71	21.80	49.36	
		5	24.02	30.25	28.16	24.02	53.50	*
		6	24.91	32.92	30.43	26.69	57.81	*
		7	26.69	34.70	37.01	28.91	64.20	*
		8	29.80	37.37	39.32	32.03	69.69	
		9	31.14	38.70	41.06	32.92	72.36	
		10	33.81	41.37	43.55	35.59	77.57	
		11	36.92	44.04	44.04	38.70	82.09	
	2	1	15.57	12.01	14.10	11.12	26.63	
		2	16.90	17.79	16.81	13.34	32.61	
		3	20.02	20.02	17.39	18.68	38.12	
		4	21.35	20.91	19.79	18.68	40.42	
		5	22.69	22.69	22.24	22.24	44.93	
		6	24.02	27.13	23.62	24.02	49.48	*
		7	24.47	27.58	26.47	23.58	51.14	*
		8	27.58	30.25	27.00	23.58	54.41	*
		9	32.92	33.36	33.72	31.14	65.60	
		10	32.92	36.48	33.36	33.36	68.12	
		11	35.59	36.92	35.85	34.70	71.54	

Table 4 Load configurations for Linerboard, units (N)

Specimen	VFM test	Load configuration	F_1	F_2	F_3	F_4	Norm(F_i)	Used for identification
1	1	1	16.90	18.24	15.88	16.46	33.78	
		2	20.02	23.13	20.73	19.57	41.81	
		3	21.80	27.13	23.44	22.69	47.70	*
		4	23.13	30.25	26.20	24.47	52.30	*
		5	27.13	35.14	33.45	27.58	62.05	*
		6	31.58	39.59	36.74	32.92	70.70	*
		7	34.70	43.59	40.70	35.14	77.43	*
		8	38.25	47.60	44.75	37.37	84.42	
		9	38.70	52.93	48.26	40.03	90.73	
		10	45.37	58.27	55.07	42.26	101.35	

Table 4 (continued)

Specimen	VFM test	Load configuration	F_1	F_2	F_3	F_4	Norm(F_i)	Used for identification
		11	48.49	60.94	57.56	44.93	106.75	
	2	1	19.57	23.58	25.18	20.91	44.83	
		2	21.80	26.24	31.14	20.91	50.70	*
		3	25.80	32.92	37.68	24.91	61.56	*
		4	28.91	38.25	43.28	28.02	70.41	*
		5	31.14	41.37	43.95	29.80	74.17	*
		6	35.59	44.93	48.53	33.81	82.36	
		7	39.14	50.26	49.69	38.25	89.39	
		8	43.15	52.04	54.58	40.92	96.04	
		9	44.93	56.05	58.00	41.37	101.17	
		10	50.26	62.28	66.59	47.60	114.47	
		11	58.27	70.28	73.17	55.16	129.35	
	1	1	22.69	22.69	20.95	23.58	44.99	
		2	28.91	30.69	26.64	26.69	56.57	
		3	28.91	31.14	29.58	27.13	58.45	*
		4	28.02	31.58	31.67	29.80	60.61	*
		5	29.80	35.59	35.94	33.81	67.74	*
		6	29.80	40.48	39.54	36.92	73.85	*
		7	35.59	42.70	41.15	38.70	79.25	*
		8	36.03	46.26	46.17	41.81	85.55	
		9	40.48	48.04	49.11	44.48	91.31	
		10	45.37	51.60	51.64	48.04	98.47	
		11	48.04	60.94	55.91	52.04	108.89	
	2	1	13.34	16.01	13.52	11.57	27.41	
		2	17.35	21.35	18.68	15.57	36.72	
		3	21.80	27.13	22.73	17.79	45.22	
		4	23.13	31.14	25.58	20.46	50.77	*
		5	27.58	34.70	29.67	23.13	58.14	*
		6	29.36	37.37	30.87	28.02	63.22	*
		7	32.47	40.48	33.32	30.25	68.69	*
		8	34.70	43.59	38.97	32.92	75.54	*
		9	35.59	50.26	42.57	36.48	83.28	
		10	39.59	53.82	49.38	40.03	92.22	
		11	42.26	57.83	51.02	43.15	97.95	
2	1	1	18.68	17.35	16.59	17.35	35.02	
		2	21.35	21.35	20.95	22.69	43.19	
		3	24.47	26.24	24.60	22.24	48.86	*
		4	27.58	30.69	29.18	26.69	57.15	*
		5	29.36	32.47	31.63	33.81	63.71	*
		6	32.92	35.14	36.92	35.59	70.34	*
		7	35.14	40.48	39.81	41.37	78.55	*
		8	40.03	42.26	41.64	43.59	83.80	
		9	44.93	47.60	47.37	48.04	94.00	
		10	49.82	50.71	52.04	52.04	102.33	
		11	53.38	58.27	56.67	54.71	111.58	
	2	1	16.01	13.79	15.75	11.12	28.60	
		2	19.13	18.24	19.13	12.46	34.92	
		3	21.35	21.80	22.55	14.68	40.68	
		4	28.91	29.36	27.58	17.79	52.68	

Table 4 (continued)

Specimen	VFM test	Load configuration	F_1	F_2	F_3	F_4	Norm(F_i)	Used for identification
		5	30.69	31.14	31.09	20.46	57.42	*
		6	32.47	33.81	35.32	23.58	63.25	*
		7	35.59	38.25	39.59	25.80	70.45	*
		8	40.03	43.15	46.22	32.03	81.40	
		9	48.04	51.15	51.96	36.92	94.80	
		10	50.71	56.49	56.14	41.81	103.26	
		11	54.27	61.83	60.99	47.60	112.93	

Table 5 Comparison of different methods for evaluating Q_{ij}; units for Q_{ij} are km^2/s^2

Material	Specimen	Test	Q_{11}	Q_{22}	Q_{12}	Q_{66}	Q_{16}	Q_{26}
Filter	1	VFM-Test1	2.59	6.16	0.92	1.34	−0.12	−0.21
		VFM-Test2	2.74	6.24	0.77	1.53	−0.08	0.16
		Ultrasonic	3.29	6.91	2.21	1.68	−0.30	−0.05[a]
		Tensile	3.09	5.13	1.31	1.47	N/A	N/A
	2	VFM-Test1	2.85	6.10	0.79	1.17	−0.07	−0.38
		VFM-Test2	2.59	7.46	1.07	1.39	−0.09	−1.10
		Ultrasonic	3.28	7.05	2.08	1.68	−0.18	−0.04[a]
		Tensile	2.98	5.70	1.35	1.53	N/A	N/A
	3	VFM-Test1	2.90	8.41	1.07	1.38	−0.05	−0.42
		VFM-Test2	3.45	6.40	1.10	1.08	0.03	−0.33
		Ultrasonic	3.24	6.94	2.34	1.68	−0.14	0.03[a]
		Tensile	3.06	5.63	1.28	2.78	N/A	N/A
Linerboard	1	VFM-Test1	4.38	12.32	1.77	2.57	−0.14	0.42
		VFM-Test2	3.82	11.86	1.43	2.75	−0.26	−0.05
		Ultrasonic	5.16	12.42	4.63	2.51	−0.11	−0.22
		Tensile	3.81	8.80	1.40	3.56	N/A	N/A
	2	VFM-Test1	6.07	13.82	2.16	3.21	−0.48	0.17
		VFM-Test2	5.16	13.66	1.91	2.71	0.16	−0.04
		Ultrasonic	5.13	12.87	4.16	2.50	−0.17	−0.10
		Tensile	3.83	9.45	1.49	3.09	N/A	N/A
	3	VFM-Test1	5.46	11.16	1.41	2.10	0.02	−0.72
		VFM-Test2	4.65	11.19	1.49	3.51	−0.46	1.67
		Ultrasonic	5.05	13.13	4.68	2.51	0.04[a]	−0.07[a]
		Tensile	5.67	8.20	1.91	2.18	N/A	N/A

[a] Not statistically different from 0 at 95 % confidence interval

References

1. Diddens I, Murphy B, Krisch M, Müller M (2008) Anisotropic elastic properties of cellulose measured using inelastic X-ray scattering. Macromolecules 41(24):9755–9759
2. Baum GA (1987) Elastic properties, paper quality, and process control. Appita J 40(4):289–294
3. Allan R (2012) The cost of paper property variation is high. Appita J 65(4):308–312
4. Yeh K, Considine J, Suhling J (1991) The influence of moisture content on the nonlinear constitutive behavior of cellulosic materials. In: Proceedings of the 1991 International Paper Physics Conference, TAPPI, Kona, Hawaii, pp 695–711
5. Haslach HW Jr (2000) The moisture and rate-dependent mechanical properties of paper: a review. Mech Time-Depend Mat 4(3):169–210
6. Castro J, Ostoja-Starzewski M (2003) Elasto-plasticity of paper. Int J Plasticity 19(12):2083–2098
7. Schulgasser K (1985) Fibre orientation in machine-made paper. J Mater Sci 20(3):859–866

8. Htun M, Andersson H, Rigdahl M (1984) The influence of drying strategies on the anisotropy of paper in terms of network mechanics. Fibre Sci Technol 20(3):165–175
9. Batten GL, Nissan AH (1986) Invariants in paper physics. Tappi J 69(10):130–131
10. Titus M (1994) Ultrasonic technology - measurements of paper orientation and elastic properties. Tappi J 77(1):127–130
11. Johnson MW Jr, Urbanik TJ (1987) Buckling of axially loaded, long rectangular paperboard plates. Wood Fiber Sci 19(2):135–146
12. Gerhardt TD (1990) External pressure loading of spiral paper tubes: theory and experiment. J Eng Mater - T ASME 112(2):144–150
13. Garbowski T, Maier G, Novati G (2012) On calibration of orthotropic elastic–plastic constitutive models for paper foils by biaxial tests and inverse analyses. Struct Multidiscip O, 1–18
14. Anurov MV, Titkova SM, Oettinger AP (2012) Biomechanical compatibility of surgical mesh and fascia being reinforced: dependence of experimental hernia defect repair results on anisotropic surgical mesh positioning. Hernia 16(2):199–210
15. Ranganathan SI, Ostoja-Starzewski M, Ferrari M (2011) Quantifying the anisotropy in biological materials. J Appl Mech - T ASME 78(6): 64,501
16. Sengupta AK, De D, Sarkar BP (1972) Anisotropy in some mechanical properties of woven fabrics. Text Res J 42(5):268–271
17. Guélon T, Toussaint E, Le Cam JB, Promma N, Grédiac M (2009) A new characterisation method for rubber. Polym Test 28(7):715–723
18. Daniel IM, Cho JM (2011) Characterization of anisotropic polymeric foam under static and dynamic loading. Exper Mech 51(8):1395–1403
19. Molimard J, Le Riche R, Vautrin A, Lee JR (2005) Identification of the four orthotropic plate stiffnesses using a single open-hole tensile test. Exper Mech 45(5):404–411
20. Boehler JP, Demmerle S, Koss S (1994) A new direct biaxial testing machine for anisotropic materials. Exper Mech 34(1):1–9
21. Edwards RL, Coles G, Sharpe WN (2004) Comparison of tensile and bulge tests for thin-film silicon nitride. Exper Mech 44(1):49–54
22. Setterholm VC, Benson R, Kuenzi EW (1968) Method for measuring edgewise shear properties of paper. Tappi J 51(5):196
23. Xavier J, Avril S, Pierron F, Morais J (2007) Novel experimental approach for longitudinal-radial stiffness characterisation of clear wood by a single test. Holzforschung 61(5):573–581
24. Xavier J, Avril S, Pierron F, Morais J (2009) Variation of transverse and shear stiffness properties of wood in a tree. Comps Part A-Appl S 40(12):1953–1960
25. Le Magorou L, Bos F, Rouger F (2002) Identification of constitutive laws for wood-based panels by means of an inverse method. Compos Sci Technol 62(4):591–596
26. Xavier J, Belini U, Pierron F, Morais J, Lousada J, Tomazello M (2013) Characterisation of the bending stiffness components of mdf panels from full-field slope measurements. Wood Sci Technol 47(2): 423–441
27. Sutton MA, Orteu JJ, Schreier H (2009) Image correlation for shape, motion and deformation measurements: basic concepts, theory and applications. Springer
28. Lyne MB, Hazell R (1973) Formation testing as a means of monitoring strength uniformity. The Fundamental Properties of Paper Related to its Uses, Transactions of the Vth Fundamental Research Symposium, Cambridge, UK, pp 74–100
29. Bruno L, Furgiuele FM, Pagnotta L, Poggialini A (2002) A full-field approach for the elastic characterization of anisotropic materials. Opt Laser Eng 37(4):417–431
30. Grédiac M, Pierron F, Surrel Y (1999) Novel procedure for complete in-plane composite characterization using a single t-shaped specimen. Exper Mech 39(2):142–149
31. Saberski ER, Orenstein SB, Novitsky YW (2011) Anisotropic evaluation of synthetic surgical meshes. Hernia 15(1):47–52
32. de Oliveira RC, Mark RE, Perkins RW (1990) Evaluation of the effects of heterogeneous structure on strain distribution in low density papers. AMD 112
33. Lappalainen T, Kouko J (2011) Determination of local strains and breaking behaviour of wet paper using a high-speed camera. Nordic Pulp Paper Res J 26(3):288–296
34. Pierron F, Grédiac M (2012) The virtual fields method: extracting constitutive mechanical parameters from full-field deformation measurements. Springer
35. Lecompte D, Smits A, Sol H, Vantomme J, Van Hemelrijck D (2007) Mixed numerical–experimental technique for orthotropic parameter identification using biaxial tensile tests on cruciform specimens. Int J Solids Struct 44(5):1643–1656
36. Furukawa T, Pan JW (2010) Stochastic identification of elastic constants for anisotropic materials. Int J Numer Meth Eng 81(4):429–452
37. Claire D, Hild F, Roux S (2004) A finite element formulation to identify damage fields: the equilibrium gap method. Int J Numer Meth Eng 61(2):189–208
38. Bonnin A, Huchon R, Deschamps M (2000) Ultrasonic waves propagation in absorbing thin plates: Application to paper characterization. Ultrasonics 37(8):555–563
39. Habeger CC (1990) An ultrasonic technique for testing the orthotropic symmetry of polymeric sheets by measuring their elastic shear coupling-coefficients. J Eng Mat - T ASME 112(3):366–371
40. Chamberlain D (2012) Industry statistics 2011. Paper Tech 53(6):20–22
41. Avril S, Grédiac M, Pierron F (2004) Sensitivity of the virtual fields method to noisy data. Comput Mech 34(6):439–452
42. Musgrave MJP (1954) On the propagation of elastic waves in aeolotropic media I. general principles. Proc Roy Soc London Ser A Math Phys Sci 226(1166):339–355
43. Musgrave MJP (1954) On the propagation of elastic waves in aeolotropic media. II. media of hexagonal symmetry. Proc Roy Soc London Ser A Math Phys Sci 226(1166):356–366
44. Jones RM (1975) Mechanics of composite materials. Taylor & Francis, London
45. Ting TCT (2000) Anisotropic elastic constants that are structurally invariant. Q J Mech Appl Math 53(4):511–523
46. Ostoja-Starzewski M, Stahl DC (2000) Random fiber networks and special elastic orthotropy of paper. J Elasticity 60(2):131–149
47. Vannucci P (2010) On special orthotropy of paper. J Elasticity 99(1): 75–83
48. Pierron F, Vert G, Burguete R, Avril S, Rotinat R, Wisnom MR (2007) Identification of the orthotropic elastic stiffnesses of composites with the virtual fields method: sensitivity study and experimental validation. Strain 43(3):250–259
49. Rossi M, Pierron F (2012) On the use of simulated experiments in designing tests for material characterization from full-field measurements. Int J Solids Struct 49(3–4):420–435